Author/s:
Li, YX;Gautam, V;Brüstle, A;Cockburn, IA;Daria, VR;Gillespie, C;Gaus, K;Alt, C;Lee, WM

Title:
Flexible polygon-mirror based laser scanning microscope platform for multiphoton in-vivo imaging

Date:
2017-11-01

Citation:
Li, Y. X., Gautam, V., Brüstle, A., Cockburn, I. A., Daria, V. R., Gillespie, C., Gaus, K., Alt, C. & Lee, W. M. (2017). Flexible polygon-mirror based laser scanning microscope platform for multiphoton in-vivo imaging. Journal of Biophotonics, 10 (11), pp.1526-1537. https://doi.org/10.1002/jbio.201600289.

Title: Flexible polygon-mirror based laser scanning microscope platform for multiphoton in-vivo imaging

Authors: Y. X. Li; V. Gautam; A. Br□stle; I. A. Cockburn; V. R. Daria; C. Gillespie; K. Gaus; C. Alt; W. M. Lee

Flexible polygon-mirror based laser scanning microscope platform for multiphoton *in-vivo* imaging

Y X Li [1,*], V Gautam[2], A Brustle[2], I A Cockburn[2], V R Daria[2], C Gillespie[2], K Gaus [3, 5], C Alt [4] and W M Lee [1, 6,†,*]

[1] *Research School of Engineering, College of Engineering and Computer Science, Australia National University, North Road, Canberra ACT 2600, Australia*

[2] *John Curtin School of Medical Research, Australian National University, Canberra City ACT 2600, Australia*

[3] *Australia- EMBL Node in Single Molecule Science, School of Medical Sciences, University of New South Wales, Sydney NSW 2052 Australia*

[4] *Wellman Center for Photomedicine, Massachusetts General Hospital, Harvard Medical School, Boston, Massachusetts 02114, USA*

[5] *Australia Research Council Centre of Excellence in Advanced Molecular Imaging, University of New South Wales, Australia*

[6] *Australia Research Council Centre of Excellence in Advanced Molecular Imaging, Australian National University, Australia*

[*] *Equal contribution*
[†] *Corresponding author: steve.lee@anu.edu.au*

Abstract: Commercial microscopy systems make use of tandem scanning i.e. either slow or fast scanning. We constructed, for the first time, an advanced control system capable of delivering a dynamic line scanning speed ranging from 2.7 kHz to 27 kHz and achieve variable frame rates from 5 Hz to 50 Hz (512 x 512). The dynamic scanning ability is digitally controlled by a new customized open-source software named *PScan1.0*. This permits manipulation of scanning rates either to gain higher fluorescence signal at slow frame rate without increasing laser power or increase frame rates to capture high speed events. By adjusting imaging speed from 40 Hz to 160 Hz, we capture a range of calcium waves and transient peaks from soma and dendrite of single fluorescence neuron (CAL-520AM). Motion artifacts arising from respiratory and cardiac motion in small animal imaging reduce quality of real-time images of single cells in-vivo. An image registration algorithm, integrated with *PScan1.0*, was shown to perform both real time and post-processed motion correction. The improvement is verified by quantification of blood flow rates. This work describes all the steps necessary to develop a high performance and flexible polygon-mirror based multiphoton microscope system for in-vivo biological imaging.

Keywords: Intravital microscopy, high-speed scanning, real-time motion correction, neuron signaling.

Introduction

In laser scanning fluorescence microscopy, the fluorescence signal time is determined by laser dwell time and characteristics of the fluorophores. While high speed imaging is often desirable for microscopy, which results in lower fluorescence signal. To increase signal in a high speed imaging system, there is often a need to either increase average laser power or acquire more frames that extends the overall acquisition time. The increase of the illuminating intensity risks saturating the fluorophores. Hence, high speed imaging systems rely on brighter fluorophores that requires fewer photons to excite. Increasing the concentration of dye-based fluorophore would lead to photo-toxicity and self-quenching. Conversely, a slow scanning system could require less frames without increasing laser power [1] and therefore could result in shorter acquisition time in total. However, for *in-vivo* imaging, a higher scanning speed is necessary for capturing fast biological events or compensate for motion artifacts. In multiphoton microscopy, the fluorescence signal is greatly dependent on the quality of the laser beams (square of the illumination intensity) that can vary for different laser scanning methods [2]. The constraints between signal-to-noise ratio and acquisition speed [1] are further complicated by the stochastic nature of the fluorescence emission. In laser scanning microscopy, there is often an optimal set of parameters that needs to be fine-tuned such as fluorophore concentration, laser scanning rate, and intensity [3-8].

Here, we focus our discussions around the laser scanning methods. Generally speaking, there are four types of laser scanning methods, namely galvanometer mirrors, resonant mirrors, polygon mirrors and acoustics optical deflectors (AOD). In commercial microscope systems, the range of scanning speeds is handled by switching between a fast and a slow mirror scanning system; termed as “tandem scanners”. Tandem scanners consist of a pair of galvanometer mirror scanner (maximum line rate ~2 kHz) and a resonant scanner of (a fixed line rate of maximum ~15 kHz) that are selected independently from each other. AOD scanners are shown to offer the

widest dynamic range of scanning speed albeit with large dispersions and aberrations [9]. Figure 1 and Table 1 show the comparison of the four types of laser scanning systems in laser scanning microscopes. We selected four independent parameters to compare: 1) scanning speed which refers to the line scanning rates, 2) scan angle indicating angle of deflection and linearity that relates to field of view, 3) efficiency which denotes the laser power transmitted across the scanner and 4) quality refers to the optical aberration and dispersion accrued after passing through the scanner. The mirror scanners (galvanometer, resonant and polygon) have a direct advantage over diffractive AOD due to their high optical efficiency. Amongst the scanning systems, polygon and AOD scanners stand out in terms of the range of scanning speeds [10]. Between these two scanners, rotating polygon scanners [11] provide a scan angle that is over two orders of magnitude larger than that of AODs. Polygon-mirror scanners [12-14] operate over a large dynamic range of scanning speeds (from 2 to 100 kHz) and retain superior optical performance over AODs. In the past, polygon-mirror laser microscopy systems [12-14] were demonstrated with basic hardware controls [15] to control rotation speeds that is not easily programmable. All in all, there has not been an advanced control module (hardware and software) that is capable of freely controlling the scanning speed selection on the fly and fully utilizes the dynamic scanning properties of polygon-mirror for multiphoton microscopy.

In this paper, we demonstrate, for the first time, the dynamic scanning properties of a polygon scanning system in a multiphoton microscope system. In contrast with past polygon-mirror microscopy systems [12-14], we provide a complete control (hardware and software, *PScan1.0* [16]) capable for freely controlling the scanning speed of polygon-mirrors and thereby vary the frames rates of the system. The system features a generic programmable signal generator (National Instruments) that rapidly transmit and receive trigger signal so as to switch between scanning speeds i.e. line rates from 2.7 kHz to 27 kHz. The programming timing system is integrated into an open-source software such that the imaging parameters such as

frame rate, field of view and pixel resolution can be digitally adjusted. This meant that the user can directly control imaging formats through a user interface for *in-vivo* imaging experiments. Although the software, *PScan1.0*, is demonstrated on a polygon-mirror scanning microscope, it is conceivable that the software can be adapted to other laser scanning microscopes. Overall, our system provides a range of scanning speeds that cannot be obtained with any current mirror-based laser scanners. In the following text, we shall outline, in detail, the complete hardware and software design followed by a series of demonstration of in-vitro and *in-vivo* imaging of biological activities such as neuron signaling in brain slices and rapid *in-vivo* blood circulation. We also carried out examples of image processing enabled through the *PScan1.0* such as denoising through frame averaging using ImageJ plug-ins and *in-vivo* motion correction (sub-pixel routines from MATLAB).

Imaging system

Hardware: optical design and electronic control

In a laser scanning microscope, the synchronization of multiple control signals between multiple devices plays a crucial role to ensure images are constructed without any aliasing. In contrast with previous polygon-mirrors that used specialized electronic control unit, we used a generic programmable signal generator that communicates at real time with a bi-cell photodiode, an analogue frame grabber, laser scanners and photon multiplier tubes (PMT) using a standard digital-analogue card (National Instruments, PCI 6110), as shown in Figure 2 (a). Analogue voltage ramps and a reference frequency signal from the card are used to control the deflection angle of the galvanometer mirrors (y-axis) and the rotation rate of the polygon scanner (x-axis) respectively. The same data acquisition card also sends a synchronization signal (VSYNC) to the frame grabber (Matrox eA/XA) [12]. The horizontal synchronization (HSYNC) is generated by a bi-cell photodiode which detects the reflected signal of polygon mirror. In the default setting, every frame has 540 vertical lines in total (38

lines are used as the front and back porch for synchronization). With a polygon scanner with 36 facets, we can achieve frame rates ranging from 5-50 Hz (512 x 512) by adjusting the line frequency from 2.7 kHz to 27 kHz. The fluorescence signal is collected by photomultiplier tubes (PMT, Hamamatsu Photonics, R928) and then amplified (Hamamatsu, C9999) before transmitting to the analogue signal inputs on frame grabber. A high voltage gain control is manually adjusted by an external controller (Sutter Instrument, PS-2).

Figure 2 (b) depicts the multiphoton microscopy that integrates a pair of orthogonal galvanometer scanning mirrors (Cambridge Technology: 6220H, 7 mm x 5 mm) and the polygon scanner (Lincoln Laser: DT-36-250-025, 4.8 mm x 5.0 mm) for providing raster scanning. All the scanning mirrors are tele-centrically conjugated to each other and share a common pupil with the objective back aperture. The imaging laser is a Ti-Sapphire pulse laser (Tsunami, Spectra Physics) that is tunable from 680-920 nm with a repetition rate of 80 MHz and approximately 150 femtoseconds pulse width at maximum 800 mW output power. The optical power is tuned using a half wave plate (HWP) with a polarization beam splitter (PBS). The beam after the HWP is first expanded by 4 times to fill the aperture of the scanning mirrors before relaying onto the back aperture of the microscope objective (MO) through 3 conjugate lens pairs. We chose an objective lens (Nikon: NIR-APO, 40x, 0.80NA/water) that has a long working distance 3.5 mm for deep tissue imaging. Based on the chosen tube lens (L10, 100 mm), the effective imaging magnification is around 20x and laser power around 15 -20 mW after the objective. The excitation wavelength is being manually tuned and monitored with by a Czerny-Turner spectrometers (CCS175/M, Thorlabs) placed close to the output of the laser. The emitted fluorescence signal is separated from the excitation light by a dichroic long-pass filter (Semrock, FF665-Di02). The emitted fluorescence is then split again by standard dichroic filter (FF562-Di03-25x36) into green and red fluorescence. Each are further filtered with emission filter (Semrock: FF01-593/40, FF01-543/22-25). The

individual fluorescence signals are collected by the two PMTs and displayed as red and green channels accordingly. Figure 2 (c) shows the experimental setup where the objective is placed in an upright position and Figure 2 (d) shows fluorescence images of clusters of 8 µm fluorescence microsphere (FocalCheck^{TM}). The inset shows a line plot of the distribution of the 8 µm beads.

Software: *PScan1.0*

In Figure 2 (e) and (f), the software architecture and graphic user interface (GUI) called *PScan1.0* is shown. *PScan1.0* was programmed and developed in MATLAB Inc. In Figure 2 (e), four primary program modules are depicted, include (1) scanning, (2) frame grabbing, (3) live-view processing and (4) data management. The scanning section of the program provides 2 counter signals and 2 analogue signals. Counter 0 generates VSYNC for the frame grabber, and counter 1 generates the reference signal for the polygon mirror drivers (BMC-7). Two analogue voltages signals are sent to galvanometer mirrors drivers (671-servo) and synchronized with the VSYNC, as depicted in Figure 2 (a). VSYNC and HSYNC signals are used to decide the frame rate and line scan rate respectively. These scanning control signals are written in LabVIEW©. *PScan1.0* uses *ActiveX* to communicate with the LabVIEW programs. Once the signals are established, the frame grabbing module sets the chosen configuration file to retrieve each frame from the frame grabber card (Matrox: Solios eA/XA). MATLAB's video processing toolbox provides several extension toolboxes that facilitate the acquisition from different frame grabbers. In this instance, *PScan1.0* calls the Matrox digital configuration files (DCF) to adjust the imaging formats through the MATLAB Matrox support package. The DCF file contains the necessary video settings such as synchronous timing, preview, frame rate, number of imaging channel and can be configured using Intellicam (built in preview program by Matrox). The imaging program can be modified to include other camera based devices. In video rate imaging, a single frame

typically contains a significant background noise that can be removed through averaging several frames. In *PScan1.0*, standard averaging routines available in ImageJ [17] are used. In addition to remove noise, *in-vivo* imaging often encounter motion artifacts because of respiratory and cardiac motion. We implemented a "sub-pixel" registration algorithm to remove the motion artifacts [18]. Finally, the acquired images are saved and converted into the respective color scheme based on the fluorescence signal, i.e. red and green, through the data management module written in MATLAB. Figure 2 (f) shows the GUI designed to provide preview images into different imaging formats. The image processing tools embedded in the GUI can be used during image acquisition to compensate motion correction [19] without relying on extensive stabilization techniques to mitigate motion [20]. Figure 3 shows the proposed method to remove lateral motion based on the image correlation. Figure 3 (a) depicts how a rapid correlation between two successive images of fluorescence images for retrieving the pixel shift between images is achieved. The shift of pixel is calculated in term of a phase value that is used to align the two images. In this way, the pixel level alignment can be implemented on-the-fly at near real-time (live preview). Figure 3 (b) illustrates an additional registration step which crops and resamples the shift at a sub-pixel level by calculating the centroid of the correlation, where all subsequent frames are used to correlate with the very initial frame. Pixel level alignment, termed here as live registration is used for live-view preview, and subpixel registration is used during post-processing after acquiring the whole image sequence.

Results

Next, we demonstrate our imaging results using the new system in fixed samples (auto fluorescence pollen grains) and the imaging of *in-vitro* neuronal activities in cultures from rat brains as well as the *in-vivo* blood flow in microvasculature of living mice. The neuronal cultures were incubated with 5 μM Cal-520AM in DMEM for 15 min prior to imaging

calcium signals at emitting fluorescence signal with wavelength of 520 nm after being excited by laser with center wavelength of 810 nm. *In-vivo* blood flow was visualized in anesthetized mice with fluorescent dye dextran either with FITC-dextran at excitation wavelength of 800 nm or Rhodamine-dextran at excitation wavelength of 850 nm. Figure 4, we show the flexibility of the high speed imaging system. Figure 4 (a) and (b) show image format with 512 x 512 pixels at 40 Hz and high resolution imaging format of 1024 x 1024 pixels at 20 Hz respectively. The increase in pixel resolution is observed by comparing digitally magnified images of fluorescence pollen grain (excitation wavelength 800 nm) captured by the imaging system as shown in the insets of Figure 4 (a) and (b). The magnified image shows that pixelation is reduced as the pixel resolution increases from 1 μm (512 x 512) to 0.5 μm (1024 x 1024). As mentioned earlier, the new control system is used to remotely control the polygon rotating speed to provide a line rate from 2.7 kHz to 27 kHz. In our system, the final pixel dwell time for 5 - 50Hz is 0.421 μs to 0.0421 μs, where additional pixels are sampled to ensure appropriate synchronization over the field of view. In Figure 4 (c), we show the exponential dependent of average fluorescence signal by changing the polygon rotation speed and imaging frame rate from 5 Hz and 50 Hz. In Figure 4 (d) and 4 (e), we show of 2 s time-averaged images of a fluorescence pollen (top) and the corresponding time series of fluorescence intensity (bottom) with 5 Hz and 50 Hz frame rates respectively (circled points in Figure 4 c). This shows that the total acquisition time to gain higher fluorescence signal for a slow scanning rate would be shorter than high speed scanning systems, without increasing laser power. The frame rate can also be changed by increasing the scanning frequency of the galvanometer scanner with smaller scan angles. In laser scanning microscopy, this means that only the frame rate of the imaging system is increased while keeping the line rate and dwell time of the laser scanning constant. This helps to mitigate any potential losses in signal to noise ratio. Figure 4 (f) shows the average

intensity versus frame rate for two separate dwell time of 0.053 μs and 0.042 μs, where the average fluorescence intensity signal maintains constant even as the scan rate change over 40-fold (20Hz to 800 Hz). However, the consequence of limiting the galvanometer scan range is the reduction of the field of view as shown in Figure 4 (g) and 4 (i) and corresponding fluorescence intensity signal over a fixed duration of 2 s. Figure 4 (h) and 4 (j) show the fluorescence signals at acquired frame rates of 320 Hz and 800 Hz respectively.

Next, we demonstrate both imaging of *in-vitro* neuronal activities in cultures from rat brains and *in-vivo* blood flow in microvasculature of living mice. The neuronal cultures were dyed with Cal-520AM for spontaneous neuronal activities imaging, and anesthetized mice were injected with fluorescent dye dextran to visualize vasculatures and measure flow rates. Figure 5 (a) shows a time averaged image from a sample of neuronal culture. Within this field of view, we selected 10 neurons and tracked their fluorescence signals over time to identify spontaneous calcium activities. Figure 5 (b) shows the corresponding time series of spontaneous calcium activity in $\Delta F/F$ from Figure 5 (a) which has 40 Hz frame rates (512 x 512). Calcium transients corresponding to action potentials in neurons occupy shorter time interval (< 5 ms) than calcium waves. Therefore, a higher temporal imaging resolution was required to discern these transient events. Hence, to record calcium transients, we switch to higher imaging speeds at frame rates of 160 Hz. The imaging system was set to acquire at 160 Hz frame rate by narrowing the field of view to 128 x 512 pixels. With high spatial and temporal resolution of the imaging system, we could measure calcium signals from soma and dendrites of neurons. Figure 5 (c) shows a zoomed-in time-averaged image of another set of cultured neurons. To justify the spatial and temporal resolution of our system for spontaneous calcium signals, which cannot be repeated, we compared the recording from a high speed imaging with a down-sampled recording. Figure 5 (d) shows raw fluorescence signals captured by the system at high speed as shown in Figure 5(d) i.e. individual frames

recorded from the selected neuron (as in Figure 5 (c), red box) at 160 Hz (thick blue) and down-sampled (thin blue)). Figure 5 (e) shows low-passed filtered signals between the two different recording speeds, which clearly indicated the advantage of high-speed imaging where distinct transient signaling states can be clearly discerned. Next, we focus on detecting calcium signals in neuronal dendrites as shown in Figure 5 (f), (g) and (h). Figure 5 (f) shows a time-average image of neurons with active dendrites (blue and red). Figure 5 (g) shows the low pass filter calcium transients signals recorded at 160 Hz from each dendrite. The signals are compared against a down sampled 40 Hz recording. Based on this data, we counted almost 200% more transient signals (32±15) transients at 160 Hz as compared to 40 Hz where around 18±15 transients are observed.

Next, we capture a series of images of vasculature close to the abdominal area of the mice where there is a large amount of cardiac and respiratory motion to test the motion correction methods of our system. Figure 6 a (i) shows a series of frames captured by the imaging system of microvasculature of a wild type mouse highlighted with fluorescent dextran-rhodamine dye. Each frame undergoes a series of cross-correlation to identify the actual pixel shifts as shown in Figure 6 a (ii). Figure 6 b (i) shows a direct time-averaging of all the frames in Figure 6 (a) that results in a blurred image. And Figure 6 b (ii) identifies the individual shift in micrometer between each frame based on cross-correlation. Here, we implemented two types of image registration; live and post-processing. In live mode, we can reference each frame to its previous frame such that any fast movement can be minimized. Based on the registration method, a large lateral shift is observed at 12 seconds into time-series in figure 6 b(ii). This shift is corrected by the registration method using the live correction method as shown in Figure 6 c (i). This shows the possibility of using live correction for tracking moving cells *in-vivo*. However, the overall longer term motion drift in the image remains. To fully remove any motion artifacts, we carried out post-processing

which is the subpixel level registration method that adds a second level correlation and alignment method at a sub-pixel. This registration method completely removes all large motion down to a sub-pixel scale as shown in Figure 6c (ii). Figure 6 d shows the overall position shifts recorded by each method. Figure 6 e (i) and Figure 6 e (ii) shows images from time-averaging of raw images and after live mode correction over period of 2 s, respectively. It shows the effectiveness of cancelling short term motion artifacts. Figure 6 f (i) and Figure 6 f (ii) show the images from time-averaging of live mode correction images and post-processing correction from the entire sequences where the sub-pixel motion correction removes all motion artifacts. Figure 6 g depicts the overall time motion correction where the live (real-time) alignment takes around 0.3 s for a 512 x 512-pixel image, which reduces the frame rate from 40 Hz to about 3 Hz during live-preview mode. A strategy to increase the frame rate is decrease galvanometer scanning area to capture with 128 x 512 thereby increasing the frame rate to about 20 Hz. For subpixel correction, the time taken is around 0.4 s which is around 33% longer than the real-time pixel level registration. Non-fluorescence red blood cells flowing in fluorescent dyed microvasculature provides a means to measure flow rates of individual blood vessels [21].

Figure 7 shows quantification of blood flow along the hind leg of fluorescein-dextran injected wild-type B6 mice. Figure 7 a shows a single frame captured at 40 Hz where two micro-vasculatures (v1 and v2) are identified and quantified. Figure 7 b (i) and b (ii) show a series of red blood cell streaks [22] from the two vasculatures which are used to quantify the blood flow rate at different time intervals from 1 to 4. The calculated velocity for the two vasculatures are displayed as a bar-plot in Figure 7 c, where there is a visual correlation of the flow rates except for interval 2. This showcases the ability of the imaging system to track different flow rates across a given field of view. However, as with any *in-vivo* flow measurements, a faster scanning with image stabilization increases the accuracy of the

measured flow. Figure 7 d, e, f and g show the single frame image of individual micro-capillaries acquired at 160 Hz and 520 Hz with the corresponding time series plot of the red blood cell streak. At 160 Hz acquisition rates, we also carried out sub-pixel motion registration, as shown in Figure 7 e (ii). Based on the streak map over three individual time intervals, we can see that the flow rates from motion correction frames differ significantly from the unregistered frames. Figure 7 f and g show a single frame image and the streak map of another capillary at higher acquisition rate of 520 Hz. Figure 7 h summaries the velocity of the capillaries at different time points. From the calculated flow, it is clearly to see that image registration increases stability of the flow measurements and the measured flow speed is around 0.01 to 0.02 mm/s slower than the unregistered measurements.

Discussion

Multiphoton microscope has been instrumental in imaging many physiological activities such as calcium signaling and hemodynamics. Calcium imaging indicates the temporal characteristic of electrical activity of cells (neurons, cardiac cells) amongst a wider neuronal network. As such, speed, resolution and field of view are all important factors to achieve high throughput imaging of neuronal networks. We have shown that an advanced polygon microscopy system easily satisfies the needs for speed, high resolution and large field of view. However, the polygon scanning mirror, much like the resonant mirrors, cannot provide vector scanning ability (target imaging sites) unlike AOD which can achieve random access points. To overcome this limitation, there is a need to introduce additional scanning mirrors or include high speed amplitude modulation for custom two dimensional patterns. Apart from calcium imaging, the ability to track changes in blood flow directions at single blood cell level provides an important clue over diseased regions in organs or energy metabolism (neurovasculature coupling). Physiological effects from respiratory and cardiac activities needs to be actively minimized either through mechanical restraints such as small mechanical

holders using thin biocompatible adhesive [23], suction [20], coverslip or software based gating i.e. simple frame rejection and gating [24] with periodic motion. Here we showed that our advanced system can efficiently implement image registration that actively realign images from all the sequences either real-time or post processed and remove errors in blood flow measurements without losing any frame. However, the limitation of software based motion correction only works well with transverse movements instead of the axial motion, which requires a further active focusing methods (tunable lenses etc).

Conclusion and future works

A fundamental parameter of laser scanning microscopy is the scanning rate of the laser scanners. Here, we demonstrate, for the first time, the tunability of a polygon-mirror laser scanning system for *in-vitro* and *in-vivo* imaging. In combination with a customized imaging program, *PScan 1.0*, we show how flexibility of the polygon-mirror is tuned to satisfy a broad range of *in-vitro* and *in-vivo* experiment requirements. We also show that our imaging program can utilize different image processing routines which demonstrates both real-time and post-processing subpixel registration of *in-vivo* images. Our work here extends the flexibility of existing range of custom-built polygon-mirror multiphoton microscope systems by integrating all the necessary hardware and software configurations onto a single imaging platform. In the future, we plan to take advantage of large scan angle of polygon-mirrors platform to develop variable acquisition over large field of view [25] so as to image various physiological phenomena.

Methods

In-vitro brain cell cultures

The neurons were isolated from hippocampal region of the brain of neonatal Wistar rats using standard procedures. The cells were cultured on glass coverslips and the recording was done after 10 days in culture. The cells were incubated with the Cal-520 AM dye (AAT

Bioquest, CA) for 15 min and recording was done in culture external medium consisting 125 mM NaCl, 3 mM KCl, 2 mM $CaCl_2$, 1 mM $MgCl_2$, 25 mM HEPES and 10 mM D-Glucose. Cal-520 AM is a calcium-sensitive dye which is preloaded onto biological cells that upon simulation signals [26]. The fluorescence intensity of Cal-520 AM increases when the concentration of calcium inside the cell increases. Harvesting of the hippocampal region of the rats follows the specified protocol approved by the Animal Ethics Committee of the Australian National University (2015/06)

Mice preparation for *in-vivo* imaging

The mice are wildtype B6 that is injected with dextran fluorescent (70 kDa) at 20% wt. Prior to imaging, mice were housed in a cage with free access to food and water, temperature/humidity control, ventilation, and regular cleaning. Ketamine/xylazine solution— Mix 1 ml of ketamine (100 mg/ml), 0.15 ml of xylazine (100 mg/ml), and 8 ml of sterile saline in aseptic condition. The mixture volume can be modified depending on the number and weight of mice. The ketamine/ xylazine solution should be prepared and used on the same day. Fluorescent dyes— Dissolve the FITC-dextran or TAMRA-dextran in sterile saline with 5% wt/vol and filter the solution through a 0.45 μm syringe filter. The solution can be aliquoted (100 μl) and stored in light-proof vials for future use. All animal experiments were performed in accordance with the guidelines and regulations of the Australian National University protocol 2016/46.

References

1. J. Vermot, S. E. Fraser, and M. Liebling, "Fast fluorescence microscopy for imaging the dynamics of embryonic development," HFSP Journal **2**, 143-155 (2008).
2. F. Helmchen, and W. Denk, "Deep tissue two-photon microscopy," Nat Meth **2**, 932-940 (2005).
3. Mikael J. Pittet, and R. Weissleder, "Intravital Imaging," Cell **147**, 983-991 (2011).
4. D. Fukumura, D. G. Duda, L. L. Munn, and R. K. Jain, "Tumor Microvasculature and Microenvironment: Novel Insights Through Intravital Imaging in Pre-Clinical Models," Microcirculation (New York, N.Y. : 1994) **17**, 206-225 (2010).
5. C. L. G. J. Scheele, C. Maynard, and J. van Rheenen, "Intravital Insights into Heterogeneity, Metastasis, and Therapy Responses," Trends in Cancer **2**, 205-216 (2016).
6. M. J. Miller, S. H. Wei, M. D. Cahalan, and I. Parker, "Autonomous T cell trafficking examined in vivo with intravital two-photon microscopy," Proceedings of the National Academy of Sciences **100**, 2604-2609 (2003).
7. C. Sumen, T. R. Mempel, I. B. Mazo, and U. H. von Andrian, "Intravital Microscopy: Visualizing Immunity in Context," Immunity **21**, 315-329 (2004).
8. S. Thiberge, S. Blazquez, P. Baldacci, O. Renaud, S. Shorte, R. Menard, and R. Amino, "In vivo imaging of malaria parasites in the murine liver," Nat. Protocols **2**, 1811-1818 (2007).
9. G. Konstantinou, P. A. Kirkby, G. J. Evans, K. M. Naga Srinivas Nadella, V. A. Griffiths, J. E. Mitchell, and R. Angus Silver, "Dynamic wavefront shaping with an acousto-optic lens for laser scanning microscopy," Opt. Express **24**, 6283-6299 (2016).
10. G. Duemani Reddy, K. Kelleher, R. Fink, and P. Saggau, "Three-dimensional random access multiphoton microscopy for functional imaging of neuronal activity," Nat Neurosci **11**, 713-720 (2008).
11. V.-F. Duma, and A. G. Podoleanu, "Polygon mirror scanners in biomedical imaging: a review," (2013), pp. 86210V-86210V-86219.
12. I. Veilleux, J. A. Spencer, D. P. Biss, D. Cote, and C. P. Lin, "Cell Tracking With Video Rate Multimodality Laser Scanning Microscopy," IEEE Journal of Selected Topics in Quantum Electronics **14**, 10-18 (2008).
13. K. H. Kim, C. Buehler, and P. T. C. So, "High-speed, two-photon scanning microscope," Appl. Opt. **38**, 6004-6009 (1999).
14. S. Choi, P. Kim, R. Boutilier, M. Y. Kim, Y. J. Lee, and H. Lee, "Development of a high speed laser scanning confocal microscope with an acquisition rate up to 200 frames per second," Opt. Express **21**, 23611-23618 (2013).
15. L. J. Mortensen, C. Alt, R. Turcotte, M. Masek, T.-M. Liu, D. C. Côté, C. Xu, G. Intini, and C. P. Lin, "Femtosecond laser bone ablation with a high repetition rate fiber laser source," Biomedical Optics Express **6**, 32-42 (2015).
16. Y. Li, and W. M. Lee, "PScan 1.0: flexible software framework for polygon based multiphoton microscopy," in *SPIE BioPhotonics Australasia*(2016), pp. 1001333-1001333-1001336.
17. C. A. Schneider, W. S. Rasband, and K. W. Eliceiri, "NIH Image to ImageJ: 25 years of image analysis," Nat Meth **9**, 671-675 (2012).
18. S. Feng, L. Deng, G. Shu, F. Wang, H. Deng, and K. Ji, "A subpixel registration algorithm for low PSNR images," in *Advanced Computational Intelligence (ICACI), 2012 IEEE Fifth International Conference on*(2012), pp. 626-630.
19. S. Lee, C. Vinegoni, M. Sebas, and R. Weissleder, "Automated motion artifact removal for intravital microscopy, without a priori information," Scientific Reports **4**, 4507 (2014).

20. M. R. Looney, E. E. Thornton, D. Sen, W. J. Lamm, R. W. Glenny, and M. F. Krummel, "Stabilized imaging of immune surveillance in the mouse lung," Nat Meth **8**, 91-96 (2011).
21. D. Kleinfeld, P. P. Mitra, F. Helmchen, and W. Denk, "Fluctuations and stimulus-induced changes in blood flow observed in individual capillaries in layers 2 through 4 of rat neocortex," Proceedings of the National Academy of Sciences **95**, 15741-15746 (1998).
22. Z. Zhong, H. Song, T. Y. P. Chui, B. L. Petrig, and S. A. Burns, "Noninvasive Measurements and Analysis of Blood Velocity Profiles in Human Retinal Vessels," Investigative Ophthalmology & Visual Science **52**, 4151-4157 (2011).
23. S. Lee, C. Vinegoni, P. F. Feruglio, and R. Weissleder, "Improved intravital microscopy via synchronization of respiration and holder stabilization," BIOMEDO **17**, 0960181-0960188 (2012).
24. S. Lee, C. Vinegoni, P. F. Feruglio, L. Fexon, R. Gorbatov, M. Pivoravov, A. Sbarbati, M. Nahrendorf, and R. Weissleder, "Real-time in vivo imaging of the beating mouse heart at microscopic resolution," Nat Commun **3**, 1054 (2012).
25. N. Ji, J. Freeman, and S. L. Smith, "Technologies for imaging neural activity in large volumes," Nat Neurosci **19**, 1154-1164 (2016).
26. M. Tada, A. Takeuchi, M. Hashizume, K. Kitamura, and M. Kano, "A highly sensitive fluorescent indicator dye for calcium imaging of neural activity in vitro and in vivo," European Journal of Neuroscience **39**, 1720-1728 (2014).

Table 1 – Single point laser scanning

	Speed (line rate)	Quality		Scan			Efficiency (Trans %)	Reported Frame rate (512X512)
		PSF	Chromatic	Linear	Angle	Speed Variable		
Galvo[24]	~ 2 kHz	Minimal	low	Yes	10-20^{o}	Yes	>90%	1-2 fps
Resonant* [24] [20]	8kHz, 12kHz, 16kHz	Minimal	low	No	12^{o}, 16^{o}, 5^{o}	No	>90%	30 fps, 40fps, 60fps
Polygon [11, 12, 14, 15]	17 kHz to ≈100 kHz	Minimal	low	Yes	20^{o} 1.8^{o}	Yes	>90%	30 fps, 200 fps
Acousto-optical deflector [10]	53kHz	Astigmatism	High	High	~0.2^{o}	Yes	~60%	115 fps

Figure 1

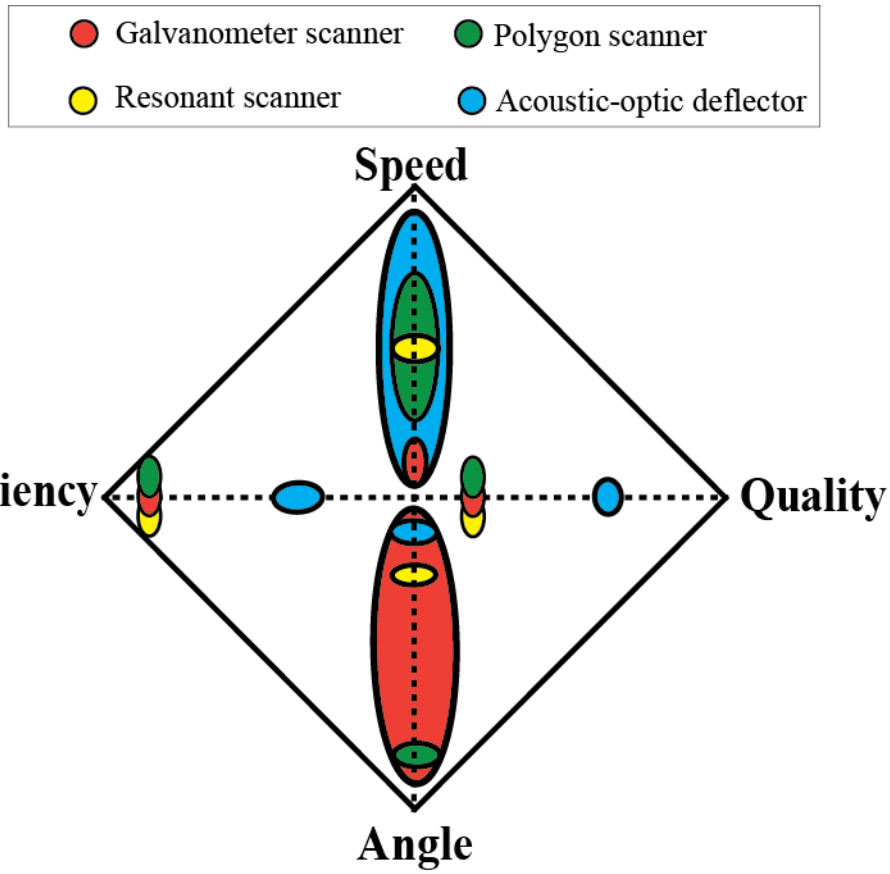

Figure 1: Comparison
Summary of laser scanning parameters (Speed, angle, quality and efficiency) as listed in table 1 (lowest to highest– center to edge), amongst the galvanometer scanner (red), polygon scanner (green), resonant scanner (yellow) and acoustic-optic deflector (blue).

Figure 2

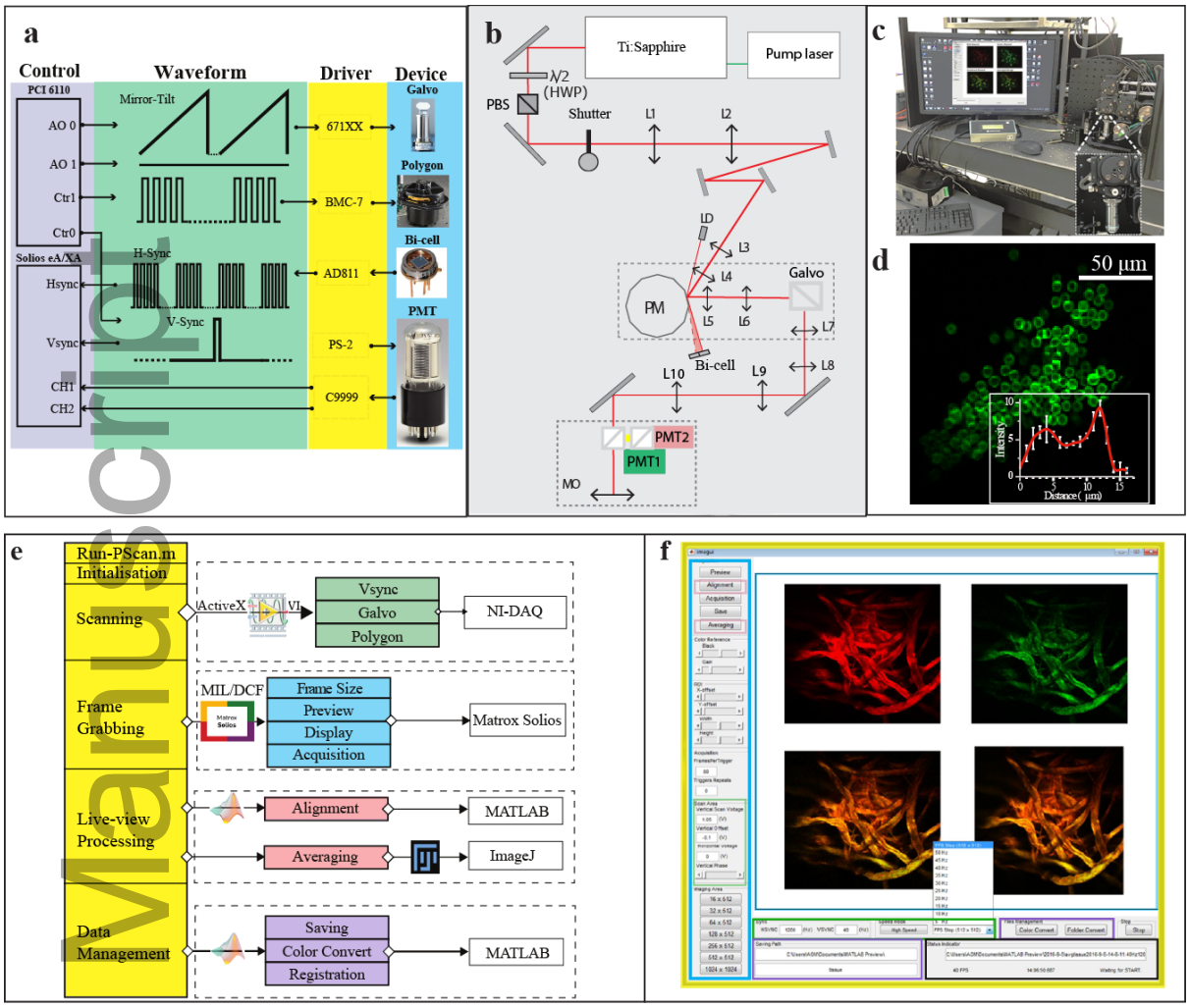

Figure 2: Hardware, optical design and software

(a) Illustrates the different voltage signals from PCI-6110 and bi-cell being transmitting between each device: frame grabber (Solios eA/XA), current amplifier onto photomultiplier tubes (PMT), polygon-mirror controller (BMC-7) and galvanometer scanning controller (671XX). (b) Polygon mirror based multiphoton microscopy with a pair of orthogonal galvanometer scanning mirrors and a polygon scanner supported by an ultrafast pulse laser (Tsunami, Spectra Physics) that emits laser with wavelength from 680-920 nm (rep rate 80 MHz, pulse width 150 femtoseconds, maximum 800 mW). The laser beam is expanded to fill the aperture of the scanning mirrors and relayed onto the back aperture of the microscope objective (MO) using several 4f systems. The emitted fluorescence signal is separated by a dichroic long-pass filter (Semrock, FF665-Di02) and standard dichroic filter (FF562-Di03-25x36) into green and red fluorescence. (c) Front image photo of imaging system. (d) Acquired sample image of FITC ring beads whose average diameter is 8 µm, the inset is the plot of the beads intensity over position. (e) Overview of the schematic of *PScan1.0* separated into four functions namely scanning, frame grabbing, live-view processing and data management as well as the individual sub-routines. (f) Graphic user interface (GUI) of *PScan1.0* that is designed to accommodate the different function in (e). (Scale bar 50 µm)

Figure 3

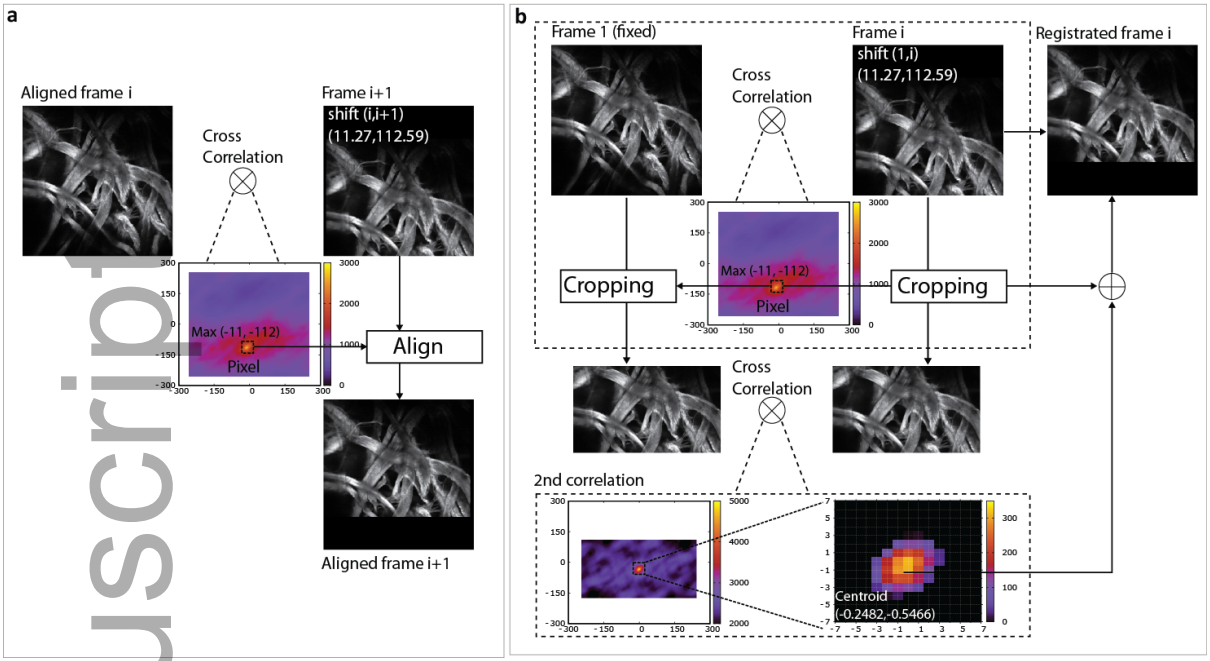

Figure 3: Image registration
(a) Flow chart of fast image alignment function for live-preview process. In this example, we set the shift as 11.27 and 112.59 in x and y axis respectively. The sample is a fluorescent tissue. *Pscan1.0* uses cross correlation between aligned frame i and unaligned frame i+1 to get the shifts and use this value the move the image back. (b) Subpixel registration in post-processing. After the cross correlation, which is the same as in the real-time alignment, *PScan1.0* uses the pixel level shifts to crop the two images and does a second cross correlation to get the centroid of shifts in subpixel level. The first frame of the video file will be set to be the fixed reference frame.

Figure 4

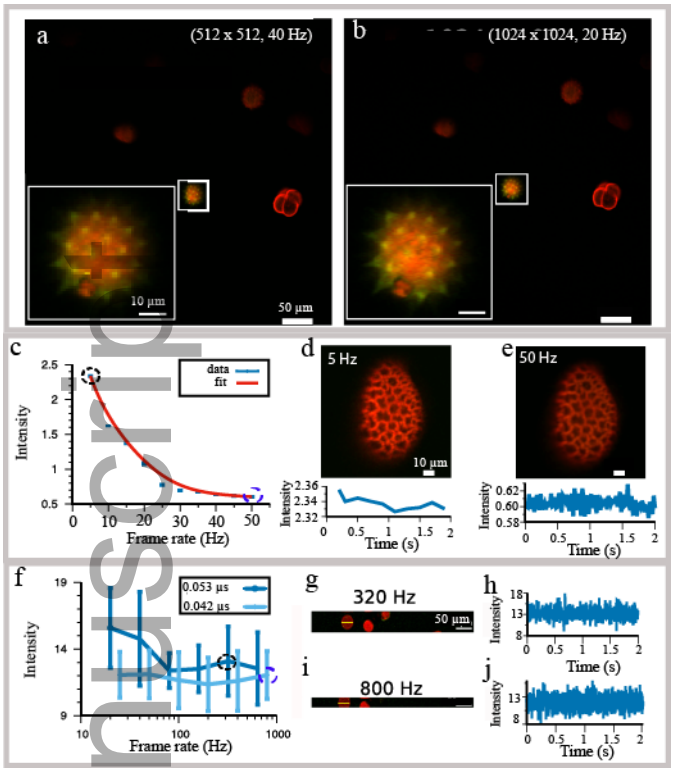

Figure 4: Imaging of fluorescence pollen grain
(a), (b) The pollen images with 512 x 512 pixels and 1024 x 1024 pixels respectively, inset shows the expanded image of the pollen sample. (c) The plot of average fluorescent intensity signal with increasing frame rate by increasing the polygon scanning rate at pixel resolution of 512 x 512. (d)-top and (e)-top show time-averaged image of pollen grain is the plot of intensity signal at 5 Hz and 50 Hz respectively (circled in (c)). (d)-bottom and (e)- bottom show the variation of intensity variation over the acquisition time. (f) Different frame rate by changing the galvanometer scanning area (slow axis) and keeping polygon scanning speed constant. (g), (h) Single frame from 320 Hz acquisition speed and intensity variation over time respectively (blue dash circle). (i), (j) Single frame from 800 Hz acquisition speed and intensity variation over time respectively (black dash circle). (Scale bar 10 µm, 50 µm)

Figure 5

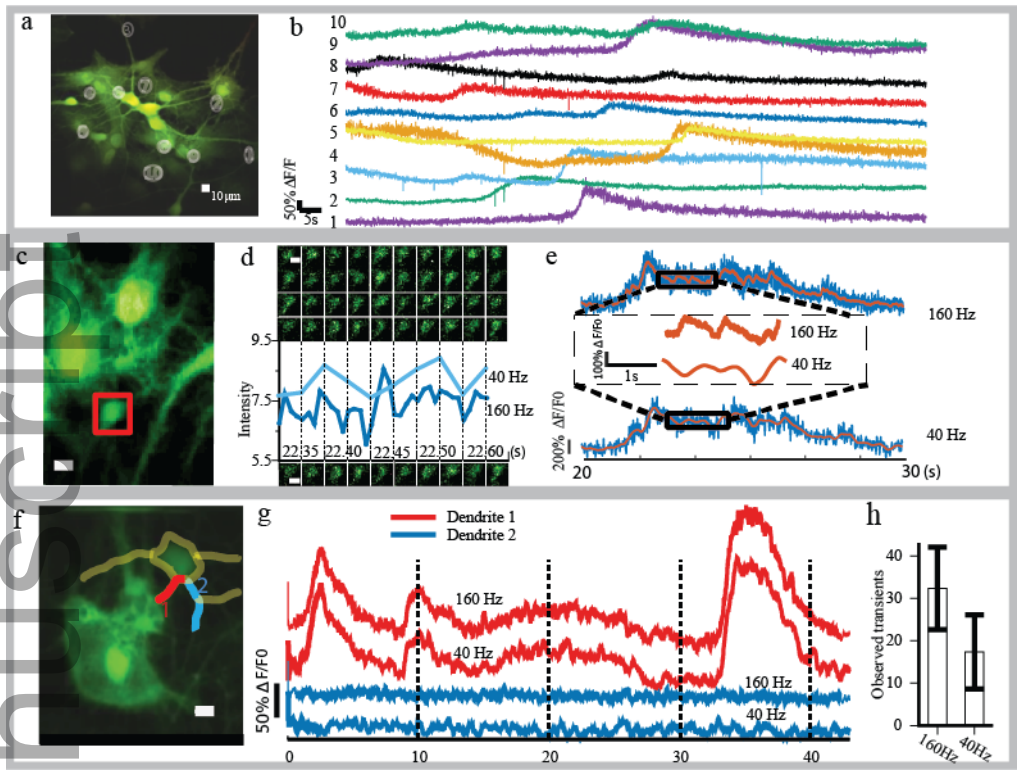

Figure 5: Imaging *in-vitro* neuronal activity from ensemble, soma and dendrite
(a) Fluorescence image of cultured rat brain cells loaded with calcium dye (CAL520AM); imaging at 512 x 512 pixels and 40 Hz frame rate. (b) 10 different regions from (a) are selected (supplementary 1) and the corresponding measurements of fluorescence are plotted with a duration of 120 s. (c) Time-averaged 160 Hz frame rate high speed imaging of neuronal soma (supplementary 2). (d) Acquired set of frames from (c) and the corresponding down-sampled 40 Hz frames. (e) Fast transient events of the neuron signal captured at 160 Hz which cannot be visualized by the down sampled 40 Hz frame rate. (f) Time-averaged image of neuronal activity imaged over 43 s at 160 Hz. (g) Calcium waves and transient peak captured by the 160 Hz and the corresponding down sampled 40 Hz data from the two selected dendrites (1-red and 2-blue). (h) Comparison of recorded number of transients between 160 Hz acquisition rate and 40 Hz rate. (Scale bars in (a), (c) and (f) are10 µm)

Figure 6

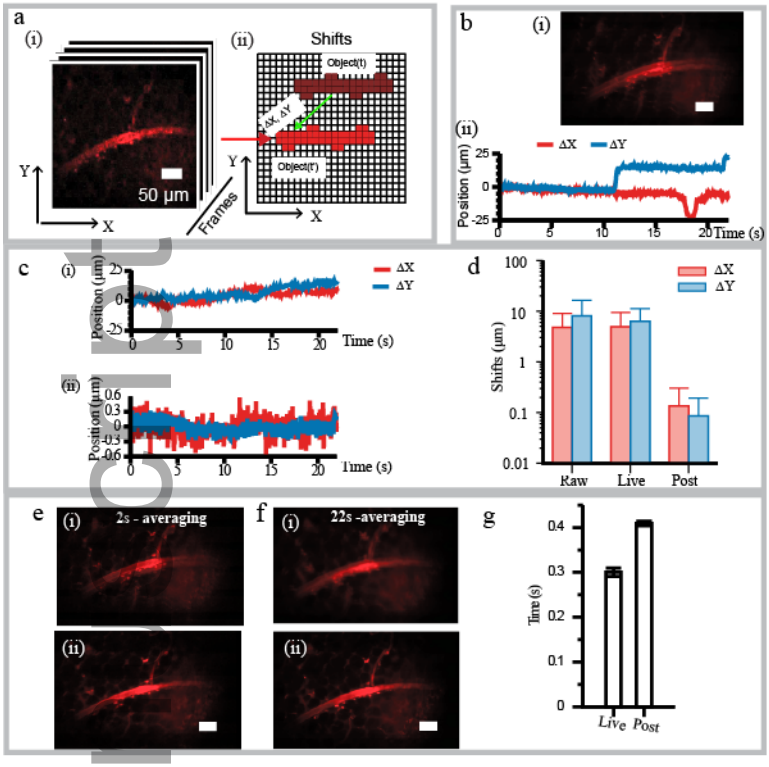

Figure 6: Image registration

a (i) A sequence of frames of a wild type mouse's microvasculature visualized with fluorescent dextran-rhodamine dye at sampling rate is 40 Hz over 22 s. a (ii) illustrates how pixel shift are calculated from each frame. b Actual pixel shift before any registration is carried out; b (i) time-averaged image over 22 s and b (ii) pixel shift over acquisition time. c (i) Pixel shift using live registration method. c (ii) Pixel shift with post-processing subpixel registration method. (d) Comparison of average position shifts over the entire length of acquisition. e (i) and e (ii) Time-averaged image over 2 s acquisition with and without live registration respectively. f(i) and f(ii) Time-averaged image over 22s acquisition time with live-registration and post-registration. (g) Time taken for live and post processing. (Scale bar 50 µm)

Figure 7

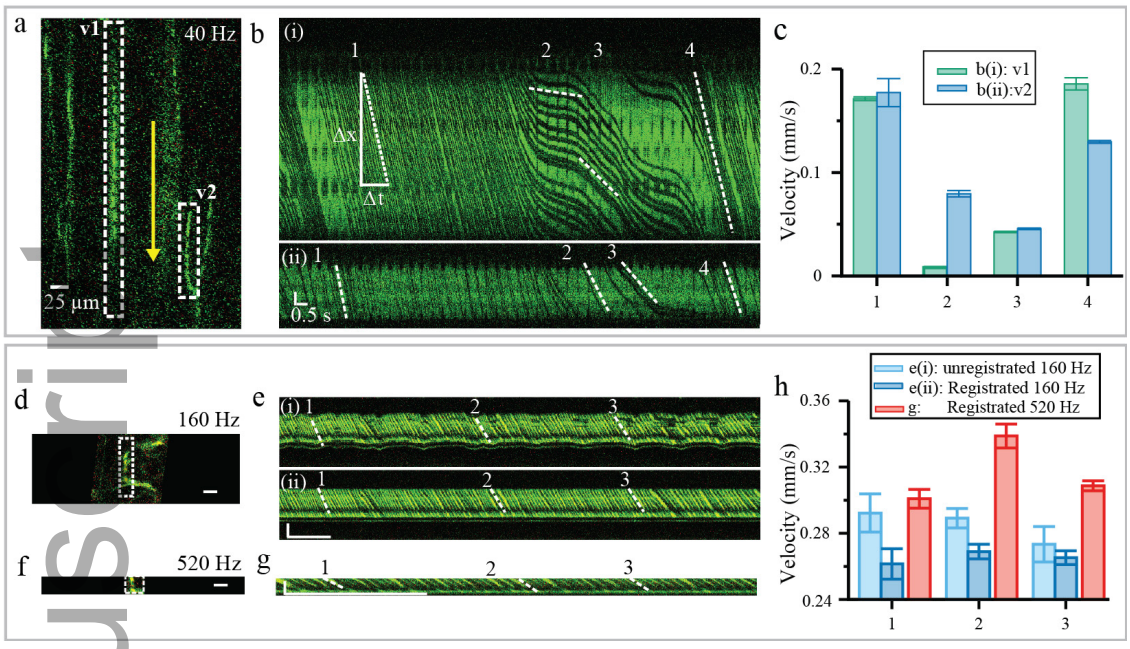

Figure 7: In-vivo measurement of flow rates of microvasculature
(a) Single frame of microvasculature with dextran-fluorescein acquired at 40 Hz. 2 vessels (v1, v2) are selected to track their flow rate. Yellow arrow indicates direction of blood flow. (b) Red blood cell streak map over the full acquisition time at vessel v1 (i) and vessel v2 (ii). (c) Calculated flow rate from (b). (d) Single frame acquired at 160 Hz. e (i) unregistered streak map of flow rates and e (ii) registered red blood cell streak map using subpixel registration (Figure 3, video in supplementary 3). (f) Single frame acquired at 520 Hz (supplementary 4). (g) Registered red blood cell streak map using subpixel registration. (h) Calculated flow rates from streak map from (e) and (g). (Scale bar, time - 0.5s, position - 25 µm)

Graphical Abstract

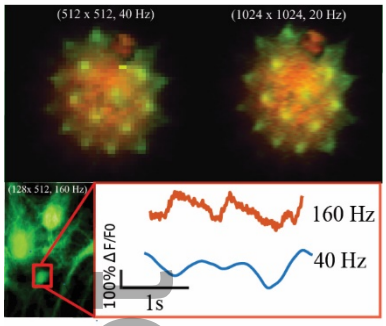

Modern multiphoton microscopy demands the smooth integration of software and hardware so as to conduct cutting edge *in-vivo* imaging at single cell level. We introduced an advanced control module capable of freely controlling scanning speed of polygon-mirror and imaging formats on-the-fly. The high dynamic scanning (ms to µs) was used to capture neuron transients and blood flow (mm/s) at single cell level over a large field of view (> 500 µm).

Supporting Information

Flexible polygon-mirror based laser scanning microscope platform for multiphoton in-vivo imaging

Y X Li, V Gautam, A Brustle, I A Cockburn, V R Daria, C Gillespie, K Gaus , C Alt and W M Lee *

Supplementary 1: Video recordings of imaging *in-vitro* neuronal activity from ensemble neuron shown in Figure. 5(a) at 40 fps

Supplementary 2: Video recordings of imaging *in-vitro* neuronal activity from soma neuron shown in Figure. 5(c) at 160 fps

Supplementary 3: Video recordings of blood flow in microvasculature shown in 7(d) at 160fps

Supplementary 4: Video recordings of blood flow in microvasculature shown in 7(f) at 520 fps